2020

Melanin deposition in two Cryptococcus species depends on cell-wall composition and flexibility

Christine Chrissian
CUNY City College

Emma Comacho
Johns Hopkins Bloomberg School of Public Health

Man Shun Fu
Johns Hopkins Bloomberg School of Public Health

Rafael Prados-Rosales
Albert Einstein College of Medicine

Subhasish Chatterjee
CUNY City College

See next page for additional authors

Melanin deposition in two *Cryptococcus* species depends on cell-wall composition and flexibility

Received for publication, November 15, 2019, and in revised form, December 31, 2019 Published, Papers in Press, January 2, 2020, DOI 10.1074/jbc.RA119.011949

Christine Chrissian[‡§1], Emma Camacho[¶], Man Shun Fu[¶], Rafael Prados-Rosales[‖], Subhasish Chatterjee[‡2], Radames J. B. Cordero[¶], Jennifer K. Lodge[‡‡], Arturo Casadevall[¶], and Ruth E. Stark[‡§ §§3]**

*From the [‡]Department of Chemistry and Biochemistry, City College of New York and CUNY Institute for Macromolecular Assemblies, New York, New York 10031, the [§]Ph.D. Program in Biochemistry and the [§§]Ph.D. Program in Chemistry, The Graduate Center of the City University of New York, New York, New York 10016, the [¶]Department of Molecular Microbiology and Immunology, Johns Hopkins Bloomberg School of Public Health, Johns Hopkins University, Baltimore, Maryland 21205, the [‖]Department of Microbiology and Immunology, Albert Einstein College of Medicine, Yeshiva University, Bronx, New York 10033, the **Department of Preventive Medicine and Public Health and Microbiology, Autonoma University of Madrid, 28049 Madrid, Spain, and the [‡‡]Department of Molecular Microbiology, Washington University School of Medicine, St. Louis, Missouri 63110*

Edited by Chris Whitfield

***Cryptococcus neoformans* and *Cryptococcus gattii* are two species complexes in the large fungal genus *Cryptococcus* and are responsible for potentially lethal disseminated infections. These two complexes share several phenotypic traits, such as production of the protective compound melanin. In *C. neoformans*, the pigment associates with key cellular constituents that are essential for melanin deposition within the cell wall. Consequently, melanization is modulated by changes in cell-wall composition or ultrastructure. However, whether similar factors influence melanization in *C. gattii* is unknown. Herein, we used transmission EM, biochemical assays, and solid-state NMR spectroscopy of representative isolates and "leaky melanin" mutant strains from each species complex to examine the compositional and structural factors governing cell-wall pigment deposition in *C. neoformans* and *C. gattii*. The principal findings were the following. 1) *C. gattii* R265 had an exceptionally high chitosan content compared with *C. neoformans* H99; a rich chitosan composition promoted homogeneous melanin distribution throughout the cell wall but did not increase the propensity of pigment deposition. 2) Strains from both species manifesting the leaky melanin phenotype had reduced chitosan content, which was compensated for by the production of lipids and other nonpolysaccharide constituents that depended on the species or mutation. 3) Changes in the relative rigidity of cell-wall chitin were associated with aberrant pigment retention, implicating cell-wall flexibility as an independent variable in cryptococcal melanin assembly. Overall, our results indicate that cell-wall composition and molecular architecture are critical factors for the anchoring and arrangement of melanin pigments in both *C. neoformans* and *C. gattii* species complexes.**

Unlike rigid walls made of bricks or stones, microbial cell walls are flexible and highly dynamic structures. Fungal cell walls undergo constant change during budding, cell growth, and yeast-to-hyphal cell transition. The fungal cell wall has such flexible viscoelastic properties that that it can allow the transit of liposomes (1). These external complex assemblies are sufficiently strong to protect the cell from the internal turgor pressure and from the outer environment, while also acting as molecular sieves that allow the intake of nutrients and the export of fungal products. Microbial cell walls are assembled from carbohydrates, proteins, and lipids in diverse architectures that depend on the fungal genus. In particular, fungal walls contain branched polysaccharides (mainly β-glucans) and mannoproteins, which are complexed with lipids, pigments, and inorganic salts (2, 3). Our current knowledge of fungal cell biology comes primarily from decades of research on model organisms such as *Saccharomyces cerevisiae*, *Schizosaccharomyces pombe*, *Candida albicans*, and *Aspergillus fumigatus*, which have laid the groundwork for studies on the cryptococcal cell wall (4–8). However, each of these organisms belongs to the ascomycetes, which have a cell-wall organization very different from that of the basidiomycetes (5, 6, 9).

Among the basidiomycetes, the genus *Cryptococcus* includes over 70 species of environmentally ubiquitous saprophytic encapsulated yeasts, of which two species complexes (10), *Cryptococcus neoformans* and *Cryptococcus gattii*, are relatively common causes of potentially fatal cryptococcal disease. *C. neoformans* is found worldwide in association with avian excreta (11, 12) or soil (13) and is the primary etiological agent of cryptococcal meningoencephalitis in immunocompromised patients (*e.g.* those infected with HIV/AIDS). On the other hand, *C. gattii* is found commonly in subtropical regions asso-

This work was supported by National Institutes of Health Grant R01-AI052733 (to A. C. and R. E. S.). The authors declare that they have no conflicts of interest with the contents of this article. The content is solely the responsibility of the authors and does not necessarily represent the official views of the National Institutes of Health.
This article contains Figs. S1 and S2.

[1] Recipient of a fellowship award from the United States Department of Education Graduate Assistance in Areas of National Need (GAANN) Program in Biochemistry, Biophysics, and Biodesign at The City College of New York (Grants PA200A120211 and PA200A150068).
[2] Present address: Dept. of Chemistry, Barnard College, Columbia University, New York, NY 10027.
[3] To whom correspondence should be addressed: Dept. of Chemistry and Biochemistry, CUNY City College of New York, MR-1024, New York, NY 10031. Tel.: 212-650-8916; Fax: 212-650-6107; E-mail: rstark@ccny.cuny.edu.

Table 1
Cryptococcal strains used in this study

Strain	Genotype	Serotype	Reference
H99	*MATα C. neoformans*	A	Toffaletti *et al.* (64)
ST211A	*C. neoformans MATα csr2::T-DNA* bearing a frameshift mutation in *CSR2*	A	Walton *et al.* (40)
R265	*MATα C. gattii*	B	Fraser *et al.* (65)
Cg53	*C. gattii MATα chs3::T-DNA (NEO)*	B	Walton *et al.* (40)

ciated with various tree species, notably eucalyptus, and causes disease primarily in immunocompetent individuals (14). Infection by both cryptococcal species is acquired by inhalation of a spore or a desiccated yeast. Thus, whether an infection is cleared, becomes latent, or progresses to cryptococcosis depends on the integrity of an individual's immune system and the *Cryptococcus* species associated with the incursion (15). From an evolutionary perspective, these cryptococcal species are thought to have diverged from a common environmental saprophyte ancestor somewhere between 30–40 (16, 17) and 100 million years ago, a time that coincided with the breakup of the supercontinent Pangea that has been proposed to have contributed to cryptococcal speciation (18). Nevertheless, they have retained extraordinarily similar microbial traits in presumed response to selective pressures in both ecological and animal niches (19). A prime example of these traits is a robust cell wall coated by a polysaccharide capsule and reinforced with melanin pigments (20–22).

Melanins are complex heterogeneous polymers of phenolic and/or indolic origin characterized by a dark color, insolubility in most solvents, and the possession of a stable free radical signature (23, 24). These natural pigments are synthesized by members of all biological kingdoms and have a wide array of functions. In the environment, melanin provides *Cryptococcus* spp. with protection against desiccation, predation by microorganisms, and UV radiation; in mammalian hosts, it alters cytokine production, offers resistance to reactive oxygen species, and diminishes phagocytosis (25–27). Whereas cryptococcal melanin is known to be composed of oligomers or polymers of cyclized catecholamines such as 3,4-dihydroxyphenylalanine (L-DOPA)[4] (28, 29), its insoluble and amorphous characteristics have hampered the elucidation of the pigment's detailed molecular architecture within the cellular milieu. Recent analyses using high resolution solid-state NMR (ssNMR) have revealed that aliphatic groups derived from cell-wall components such as polysaccharides (*e.g.* chitin) serve as a scaffold for the progressive incorporation of melanin pigments into the cryptococcal cell wall (30, 31). Furthermore, the identity of the melanin precursor (norepinephrine, epinephrine, methyl-L-DOPA, L-DOPA) alters the pigment structure as well as the polysaccharide- and lipid-based cellular scaffold associated with its deposition (32, 33). These analyses dovetail with previous reports in other fungi (34–36) as well as in insects (37), where an intimate association between melanin and the chitin polysaccharide was described. Conversely, several studies using both *C. neoformans* and *C. gattii* demonstrated that strains defective in the chitin/chitosan biosynthetic machinery are unable to retain melanin within the cell wall, thus yielding a "leaky melanin" phenotype characterized by visual detection of the pigment in the culture medium or agar surrounding the cells (38–40).

In the present work, we employ magic angle spinning (MAS) ssNMR assisted by isotopically labeled reagents and other supporting biochemical techniques to focus on the cell-wall structure of the two most clinically relevant cryptococcal isolates: *C. neoformans* H99 and *C. gattii* R265. Our results demonstrate that both polysaccharides, and particularly chitosan, together with lipids, play critical roles in anchoring and layering melanin within the cryptococcal cell wall.

Results

Melanized yeast cells of C. gattii R265 display notably augmented and condensed deposition of the pigment within the cell wall

Upon light microscopy examination of melanized cells from two isolates representing the *C. neoformans* and *C. gattii* species complexes, H99 and R265, respectively (Table 1), we observed that a subset of *C. gattii* R265 cells displayed highly pigmented cell walls, which were not observed for *C. neoformans* H99 (Fig. 1). The mean cell body and capsule sizes were also observed to differ between the two species (Fig. S1). Multiple studies have established that the molecular architecture of the *C. neoformans* cell wall directly influences the deposition and retention of melanin pigments (31, 38, 39, 41–43). Consequently, we tested the generality of cell-wall ultrastructural characteristics associated with melanin deposition by using transmission EM to further compare the melanized cell walls of *C. neoformans* H99 with *C. gattii* R265, which is a strain from the VGIIa molecular subtype reported to exhibit robust melanin production at 37 °C (44–46). We observed significant differences in the ultrastructural properties of *C. neoformans* H99 and *C. gattii* R265 (Fig. 2). Transmission EM revealed that the *C. neoformans* H99 melanized cell wall had a heterogeneous pigment distribution characterized by multiple layers of variable electron density (Fig. 2*A*, *top*), which is consistent with previous studies conducted by our group (42). In contrast, the melanin pigments embedded in *C. gattii* R265 cell walls were found to be more uniformly distributed, forming just two highly electron-dense layers that closely surrounded the cell body (Fig. 2*A*, *bottom*). The melanized cell walls of *C. gattii* R265 cells were additionally observed to have a significantly smaller thickness compared with *C. neoformans* H99 (Fig. 2*B*), a finding that

[4] The abbreviations used are: L-DOPA, 3,4-dihydroxyphenylalanine; ssNMR, solid-state NMR; MAS, magic angle spinning; DPMAS, direct polarization magic angle spinning; CPMAS, cross-polarization magic angle spinning; TEDOR, transferred echo double resonance; DARR, dipolar-assisted rotational resonance; MBTH, 3-methyl-2-benzothiazolone hydrazine hydrochloride; DPBS, Dulbecco's PBS; MM, minimal medium; SPINAL, small phase incremental alternation pulse sequence; rf, radiofrequency field; 1D and 2D, one- and two-dimensional, respectively.

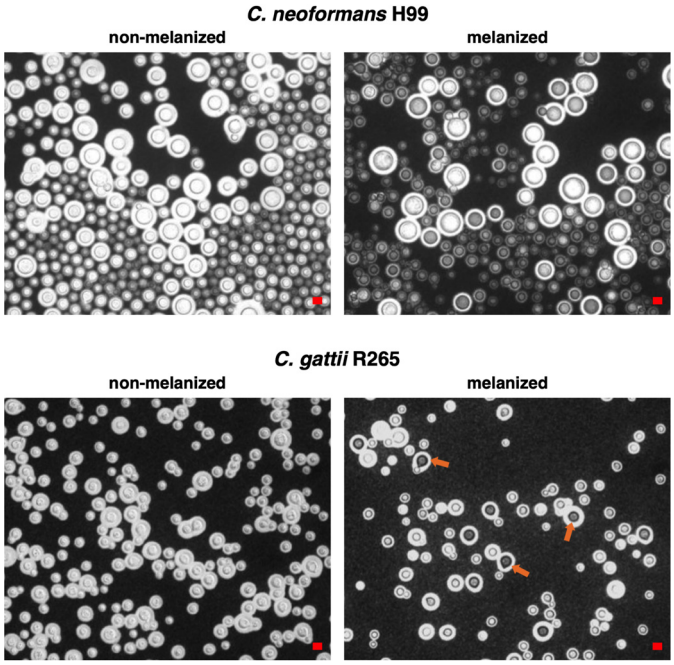

Figure 1. A subset of *C. gattii* R265 melanized cells exhibit highly pigmented cell walls. Shown are representative images of nonmelanized and melanized yeast cells of *C. neoformans* H99 and *C. gattii* R265 visualized by light microscopy using India ink counterstaining. Over 300 cells were counted at ×40 magnification in five different fields. Highly melanized *C. gattii* R265 cells showing enhanced cell-wall pigmentation (*red arrows*) corresponded to 7.5% of the total. *Scale bar*, 10 μm.

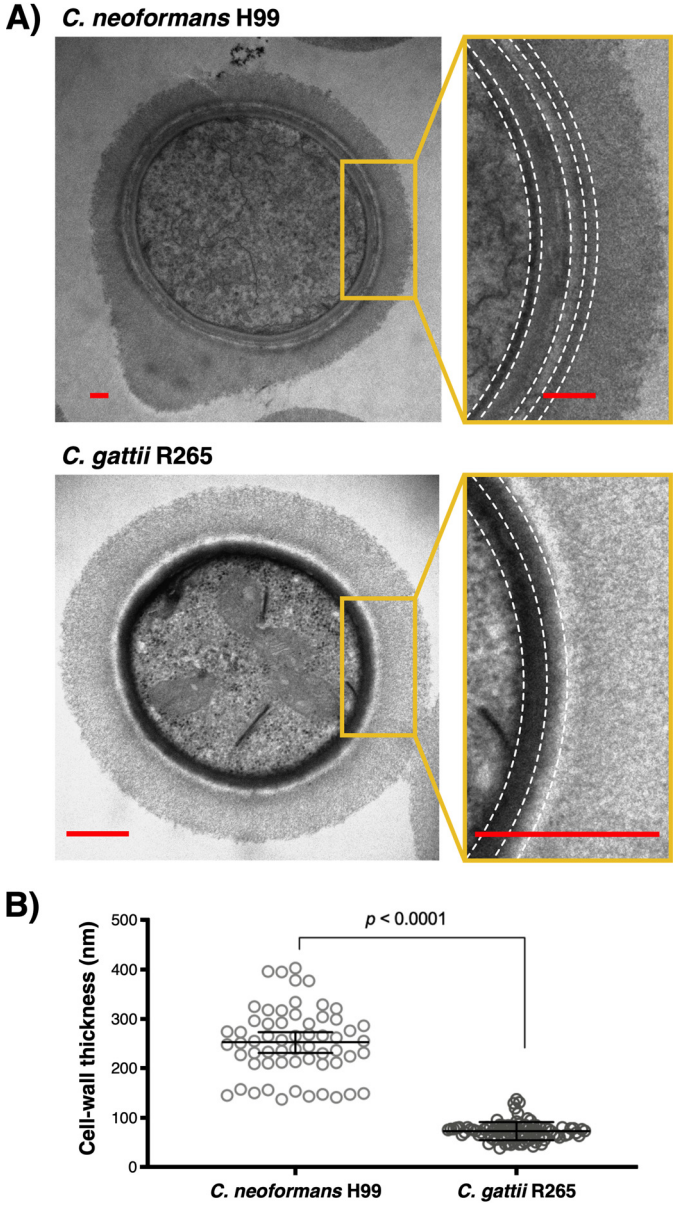

Figure 2. The melanized cell wall of *C. gattii* R265 reveals a compact and uniform deposition of melanin pigments. *A*, representative cross-sectional transmission electron micrographs of *C. neoformans* H99 (*top*) and *C. gattii* R265 (*bottom*) melanized yeast cells. The *magnified images* show a *close-up view* of the cell wall with *dashed lines* to illustrate the difference in layered melanin pigment arrangement between these two cryptococcal isolates, possibly attributable to their cell-wall chitinous compositions. *Scale bar*, 500 nm. *B*, measurement of *C. neoformans* H99 and *C. gattii* R265 melanized cell-wall thickness. Data were obtained by measuring 12–18 cells per strain (5 measurements/cell) and analyzed using the Mann–Whitney test, two-tailed *p* value with 99% confidence level. *Error bars*, 95% confidence interval of the median.

could be attributed to the compact arrangement of their melanin pigments.

Interestingly, the phenotype displayed by *C. gattii* R265 cells was similar to that observed in *C. neoformans* H99 cells supplemented with GlcNAc (42). Prior work by our group demonstrated that *C. neoformans* H99 cells grown in the presence of 1 or 5 mM GlcNAc displayed a more uniform arrangement of cell-wall melanin pigments as well as diminished cell-wall and cell-body diameters compared with nonsupplemented control cells (42). We hypothesize that these morphological changes result from differences in the cell-wall composition of *C. gattii*, in analogy with GlcNAc-supplemented *C. neoformans* H99 cells that were found to have a relatively larger amount of cell-wall chitosan than controls. Therefore, our current results suggest that the chitinous composition of *C. gattii* R265 cell walls could favor enhancement of melanin deposition in a condensed and uniform manner.

The "leaky melanin" phenotype is associated with decreased levels of chitosan in both C. neoformans and C. gattii mutant strains

The leaky melanin phenotype refers to the observation that some *Cryptococcus* spp. mutants appear unable to retain melanin in the cell wall and instead release the pigment into the culture medium exterior to the cell (38, 39). To test the proposed correlation of melanin deposition and retention with chitinous molecular composition in *C. gattii* R265 melanized fungal cells, we conducted a biochemical measurement of chitin and chitosan content using the 3-methyl-2-benzothiazolone hydrazine hydrochloride (MBTH) colorimetric assay, as reported previously in GlcNAc-supplemented *C. neoformans* H99 cells (42). As hypothesized above, the cell-wall chitosan content of *C. gattii* R265 WT cells was found to be nearly 3-fold greater than in *C. neoformans* H99 WT cells (Fig. 3*A*). Although the change in the chitin/chitosan ratio associated with this increase was not statistically significant (Fig. 3*B*), *C. gattii* R265 cell walls also contained a relatively higher overall amount of total chitinous material (chitin plus chitosan) than *C. neoformans* H99 (Fig. 3*A*).

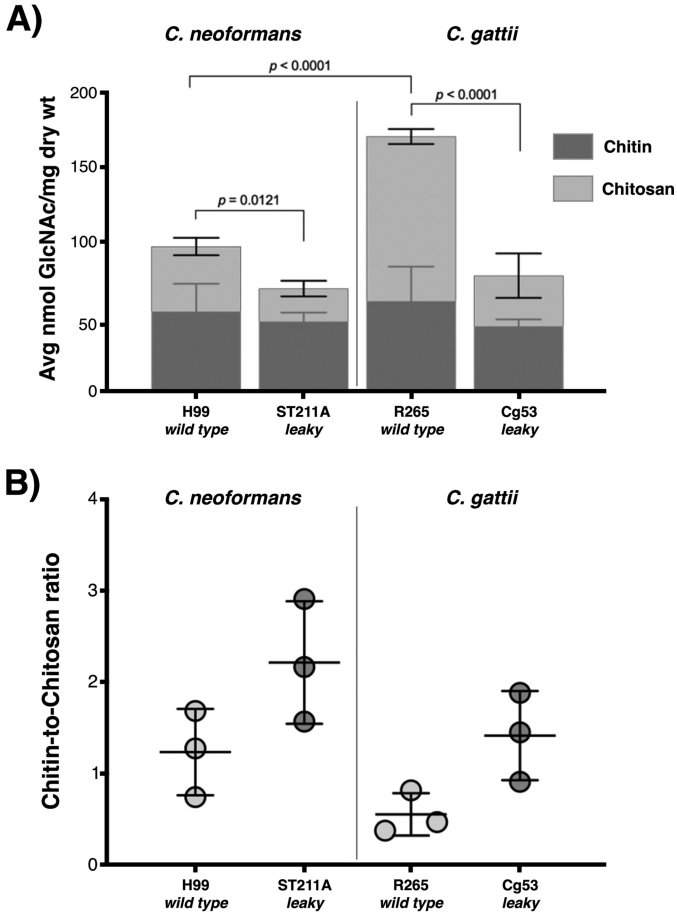

Figure 3. Cryptococcal strains defective in the retention of cell-wall melanin exhibit decreased levels of cellular chitosan. *A*, biochemical determination of chitin and chitosan using the MBTH colorimetric reaction measured at 650 nm. Reduction in the cell-wall content of chitinous polysaccharides, primarily attributable to chitosan contribution, is associated with the leaky melanin phenotype in both *C. neoformans* ST211A and *C. gattii* Cg53 strains. Analysis of variance with a Bonferroni post hoc test indicated significant differences between groups. *B*, chitin/chitosan ratio. A boost in the chitin/chitosan ratio correlates with the leaky melanin phenotype independently of the *Cryptococcus* species. All data represent an average of three independent biological experiments. *Error bars*, S.D.

To further investigate whether a reduction in chitosan content was responsible for compromised pigment retention in both *Cryptococcus* species, we assessed the cell-wall chitin and chitosan content of two other leaky melanin strains previously identified for *C. neoformans* and *C. gattii*, ST211A and Cg53, respectively (40). The ST211A mutant has a frameshift in the *CSR2* gene (GenBank™ accession number MK609896),[5] along with a T-DNA insertion elsewhere in the genome. The Cg53 mutant has a T-DNA insertion in the *CHS3* gene; the phenotype was complemented by transformation with a WT *CHS3* gene. Chs3 is a chitin synthase that is an integral membrane protein, and Csr2 is an accessory protein to chitin synthase, which is membrane-associated likely via a C-terminal prenyl group (39). Both genes have been shown to be required for chitosan production in *C. neoformans*, and these two proteins have been hypothesized to form a membrane-bound complex that synthesizes the chitin that is then converted to chitosan (39). Whereas absolute levels of chitin were found to be similar for all four strains, including parent and leaky mutants, the chitosan absolute and proportional content for both the *C. neoformans* ST211A and *C. gattii* Cg53 mutants exhibited significant reductions compared with their respective parent strains (Fig. 3*A*) and, consequently, higher chitin/chitosan ratios (Fig. 3*B*). Interestingly, the lowered chitosan level of the *C. gattii* Cg53 mutant resulted in a chitin/chitosan ratio similar to that of *C. neoformans* H99, suggesting a dependence of aberrant pigment retention on other compositional or structural changes of the scaffold. These findings suggest that diminished cell-wall chitosan content may be a feature common to cells from leaky mutant strains regardless of the *Cryptococcus* species, underscoring the likely importance of this polysaccharide for anchoring of melanin to the cryptococcal cell wall. Moreover, these data support the contention that the phenotypic traits shared by melanized *C. gattii* R265 and GlcNAc-supplemented *C. neoformans* H99 cells are due to increased cell-wall chitosan content, which could promote uniform melanin pigment deposition and consequently result in diminished cell-wall thickness.

The condensed pigment arrangement in melanized C. gattii R265 yeast cells does not result in increased melanin deposition

In our prior work, supplementation with GlcNAc was determined to augment the chitin/chitosan ratio of *C. neoformans* H99 cells, and increased levels of chitosan were correlated with greater cell-wall pigment deposition and retention, as evidenced by a greater mass yield of melanin ghosts with a relatively higher pigment content than nonsupplemented cells (42). Melanin ghosts are fungal pigment structures isolated via a degradative process that includes treatment with hot acid. Nevertheless, due to the insoluble and recalcitrant nature of melanin, a variety of cellular remnants remain associated with the pigment, resulting in structures that resemble hollowed-out yeast cells and thus are referred to as "melanin ghosts." The relative pigment content of melanin ghost samples can be estimated using ssNMR spectroscopy and serves as a measure of fungal melanin deposition.

Thus, to determine whether the substantial chitosan content of *C. gattii* R265 is associated with increased cell-wall pigment deposition, quantitatively reliable ^{13}C direct polarization magic angle spinning (DPMAS) spectra were acquired for melanin ghosts isolated from both *C. neoformans* H99 and *C. gattii* R265 cells. The relative content of indole-based pigment was estimated by comparing the aromatic region peak area (*shaded*) with the total signal area of each spectrum. Interestingly, aromatic signals comprised 35% of the *C. neoformans* total spectral area, whereas only 30% of the *C. gattii* melanin ghost total signal intensity was attributable to the pigment (Fig. 4*A*). Furthermore, *C. neoformans* H99 yielded a greater dry mass of melanin ghosts than *C. gattii* R265 (20.7 mg *versus* 16.6 mg, respectively) (Fig. 4*B*). In the context of our other data, this finding indicates that the condensed pigment deposition exhibited by *C. gattii* R265 melanized cell walls does not translate into an overall increase in its content.

[5] A. Idnurm, personal communication.

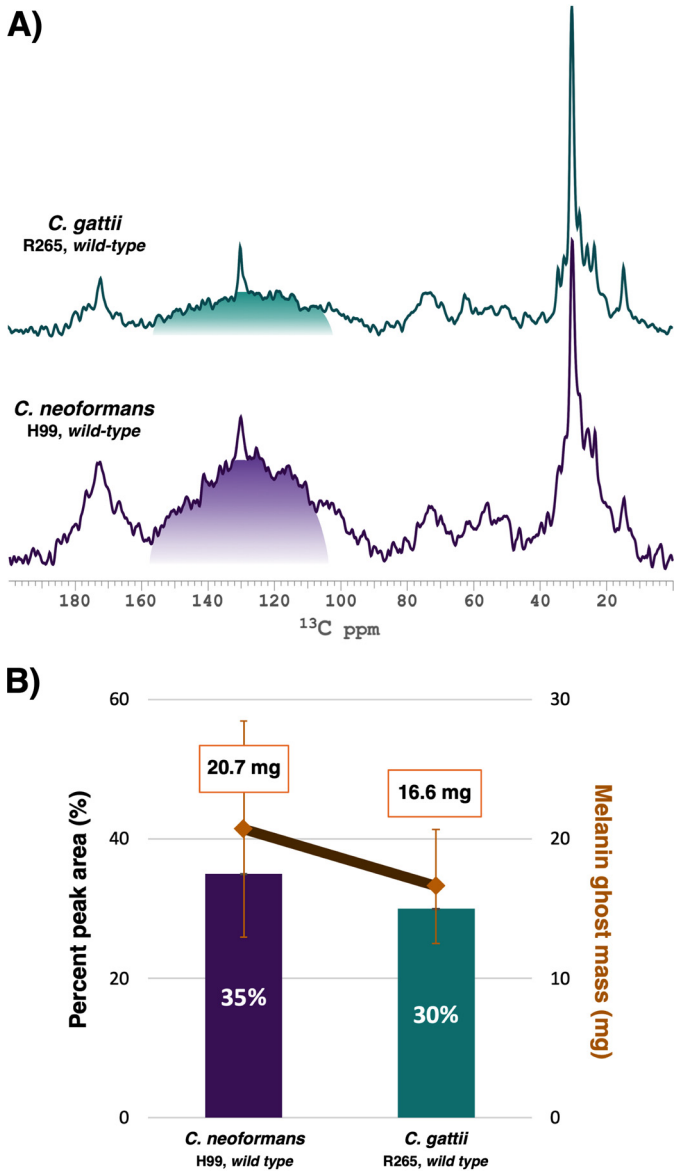

Figure 4. *C. neoformans* H99 yields a greater mass of melanin "ghosts" with a relatively higher pigment content than *C. gattii* R265. *A*, representative 1D ^{13}C DPMAS spectra of melanin ghosts generated from *C. neoformans* H99 and *C. gattii* R265 parent strain cell cultures. The *shaded region* (110–160 ppm) represents the relative contribution of signal intensity attributable to the indole-based melanin pigment. The peak at ~130 ppm arises from the unsaturated carbons of fatty acids and thus was excluded from the *shaded region*. *B*, estimation of pigment content relative to retained cellular constituents obtained from quantitatively reliable ^{13}C DPMAS spectra (*bar graph*) and measurement of melanin ghost mass (*line graph*). The data represent the mean of results from three independent trials. The S.D. from the mean was less than 0.01% for the relative aromatic pigment content measurements, and thus the *error bars* are too small to be visible. *Displayed error bars*, S.D. from the mean melanin ghost mass generated from each isolate.

Lipid and polysaccharide constituents are retained differentially in leaky melanin ghosts and with species-specific relative compositions

In light of our finding that the *C. gattii* leaky mutant Cg53 had a chitin/chitosan ratio similar to that of the *C. neoformans* H99 strain, we sought a more comprehensive accounting of the compositional and architectural factors that distinguish the parent and leaky mutant strains of each *Cryptococcus* species. A quantitative ^{13}C solid-state NMR analysis was carried out for melanin ghosts generated from cell cultures containing uniformly ^{13}C-enriched glucose as the sole carbon source and natural-abundance L-DOPA as the obligatory melanization precursor. Because cryptococcal species are unable to synthesize melanin pigments from nutrient sources (47), the provision of [U-^{13}C]glucose results in selective incorporation of the stable ^{13}C isotope into glucose-derived nonpigment moieties. Thus, the resulting spectra display signals attributable solely to the aliphatic constituents that survive the degradative melanin ghost isolation protocol (Fig. 5). This strategy allowed us to estimate the relative amounts of long-chain lipid, polysaccharide, and "other" nonpigment components in these melanin ghost samples by acquiring quantitatively reliable ^{13}C DPMAS spectra and comparing peak integrals expressed as fractions of the total integrated NMR signal intensity across the spectrum. The constituents retained by the ghosts should then reflect the adherence of the pigment and the architectural features that offer protection from chemical and enzymatic degradation.

Upon visual inspection, the spectra of the four [U-^{13}C]glucose-labeled melanin ghost samples appeared largely similar: they each displayed signals corresponding to cell-wall polysaccharides (~55–105 ppm) as well as saturated and unsaturated long-chain methylene carbons (~30 and 130 ppm, respectively) (Fig. 5*A*). However, quantitative analysis revealed considerable compositional differences among the four strains. Although resonances consistent with long-chain fatty acids ($(CH_2)_n$ and CH_3) that are primarily attributable to triacylglycerides[6] accounted for the majority of signal intensity in each spectrum, their relative contributions in WT parent *versus* mutant strains exhibited opposite trends for the two *Cryptococcus* species. Whereas the melanin ghosts isolated from the *C. neoformans* ST211A leaky strain were slightly poorer in lipids than H99 (60% *versus* 68%), *C. gattii* Cg53 leaky ghosts had a greater proportion of lipids compared with the R265 sample (73% *versus* 62%) (Fig. 5*B*).

The peaks corresponding to polysaccharide carbons contributed only a minor proportion of the overall signal intensity in each spectrum. In *C. neoformans*, the relative polysaccharide content was essentially invariant for melanin ghosts isolated from H99 *versus* ST211A mutant cells (8.5% *versus* 7.3%). Both samples displayed similar lipid/polysaccharide ratios (8.1 *versus* 8.2 for parent and mutant, respectively) despite the diminished lipid percentage in the ST211A ghosts. Interestingly, the most substantial difference between the parent and leaky *C. neoformans* samples was the relative contribution of constituents other than long-chain methylenes or polysaccharides (23% *versus* 33%) (Fig. 5*B*). The ST211A melanin ghost sample displayed a visibly greater percentage of signal intensity in the "other" spectral region between ~110 and 160 ppm than the H99 sample. Sharp peaks appearing in this chemical shift range are typically attributable to double-bonded carbons from unsaturated fatty acid chains, and thus, the ~130 ppm resonances are categorized as lipids. However, the broad underlying components in this spectral region suggest a collection of relatively rigid, less motionally averaged conjugated moieties that are currently unassigned and under further investigation.

[6] C. Chrissian, unpublished observations.

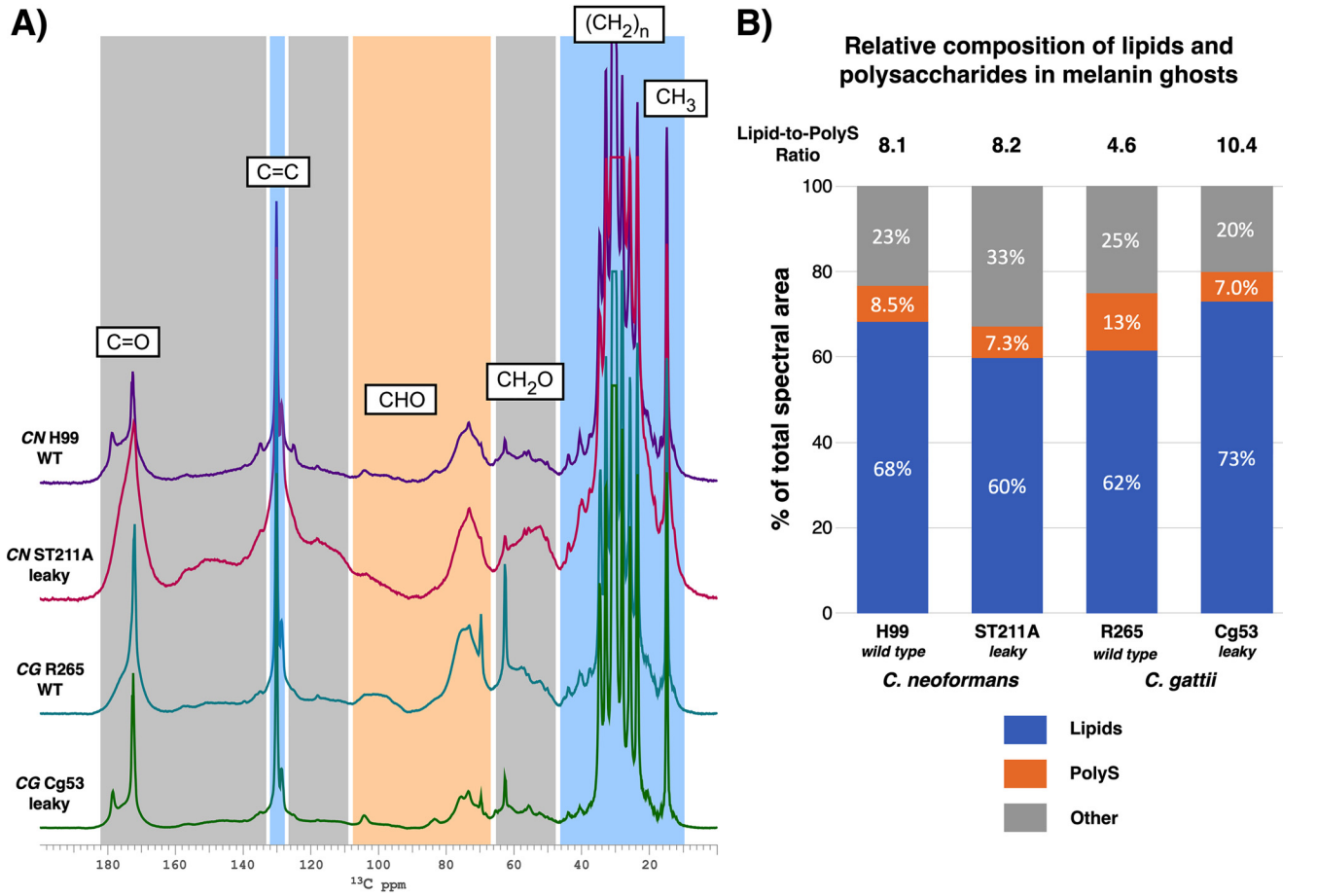

Figure 5. The relative composition of retained cellular constituents differs between *C. neoformans* and *C. gattii* leaky mutant and parent strain melanin ghosts. *A*, 1D ^{13}C DPMAS spectra of melanin ghosts generated from *C. neoformans* and *C. gattii* parent and leaky melanin strain cell cultures containing D-[U-$^{13}C_6$]glucose as the sole carbon source. *B*, measurement of each cellular constituent type relative to the total amount of retained nonpigment moieties obtained from quantitatively reliable ^{13}C DPMAS spectra. *PolyS*, polysaccharide. Each spectrum is normalized by setting the largest peak to full scale. The top of the largest peak was cropped to improve the visibility of smaller peaks.

Despite the modest quantitative contributions of polysaccharide carbon signals apparent in both *C. neoformans* spectra, the polysaccharide proportion in *C. gattii* was nearly 2-fold greater in R265 ghosts compared with the Cg53 mutant (13% *versus* 7.0%). The compositional differences between the two *C. gattii* samples are further underscored by the significantly higher lipid/polysaccharide ratio of Cg53 (10.4, compared with 4.6 for the parent strain), which results from concurrently increased lipid and decreased polysaccharide levels. Thus, from a compositional perspective, our ^{13}C NMR measurements revealed that leaky melanin phenotypes could result from a mix of constituent classes that is particular to the *Cryptococcus* species: elevated "other" materials comprising unidentified aromatic ring structures for *C. neoformans* or an enhanced lipid/polysaccharide ratio for *C. gattii*.

Two-dimensional (2D) ^{13}C-^{15}N NMR spectroscopy establishes chitin and chitosan as glucose-derived constituents retained by melanin ghosts

Although the MBTH assay provided a practical means to correlate changes in chitin/chitosan ratios with the leaky melanin phenotype in both *Cryptococcus* species, this approach is not practical for melanized fungal samples and falls short of revealing the macromolecular architecture of these polysaccharides within the underlying cellular scaffold. Moreover, the recalcitrant nature of melanin would require very harsh chemical or enzymatic procedures to isolate the pigment-associated cellular constituents from ghost samples, risking hydrolysis in an effort to achieve identification and characterization. Instead, we have previously used solid-state 2D ^{13}C-^{13}C NMR of [U-^{13}C]glucose-labeled ghosts to obtain ^{13}C chemical shifts and structural connections that implicate the acetyl group of chitin (31). Although chitosan lacks distinctive carbon-containing structural features that could distinguish it from the multitude of other moieties present in ^{13}C NMR spectra of melanin ghosts, along with chitin it is unique among polysaccharides in possessing nitrogenous functional groups. Thus, we prepared melanized *C. neoformans* H99 cell cultures containing [U-^{13}C]glucose and [^{15}N]glycine as the sole carbon and nitrogen sources, respectively, to verify that chitosan and chitin were components of the melanized cell-wall scaffold. ^{15}N NMR spectra of the ghosts (Fig. S2) displayed signals from chitin (123 ppm) and chitosan (35 ppm) (48, 49), and definitive identifications could be made from 2D ^{13}C-^{15}N transferred echo double resonance (TEDOR) experiments that identify spatially proximal ^{13}C-^{15}N pairs (Fig. 6) (50, 51).

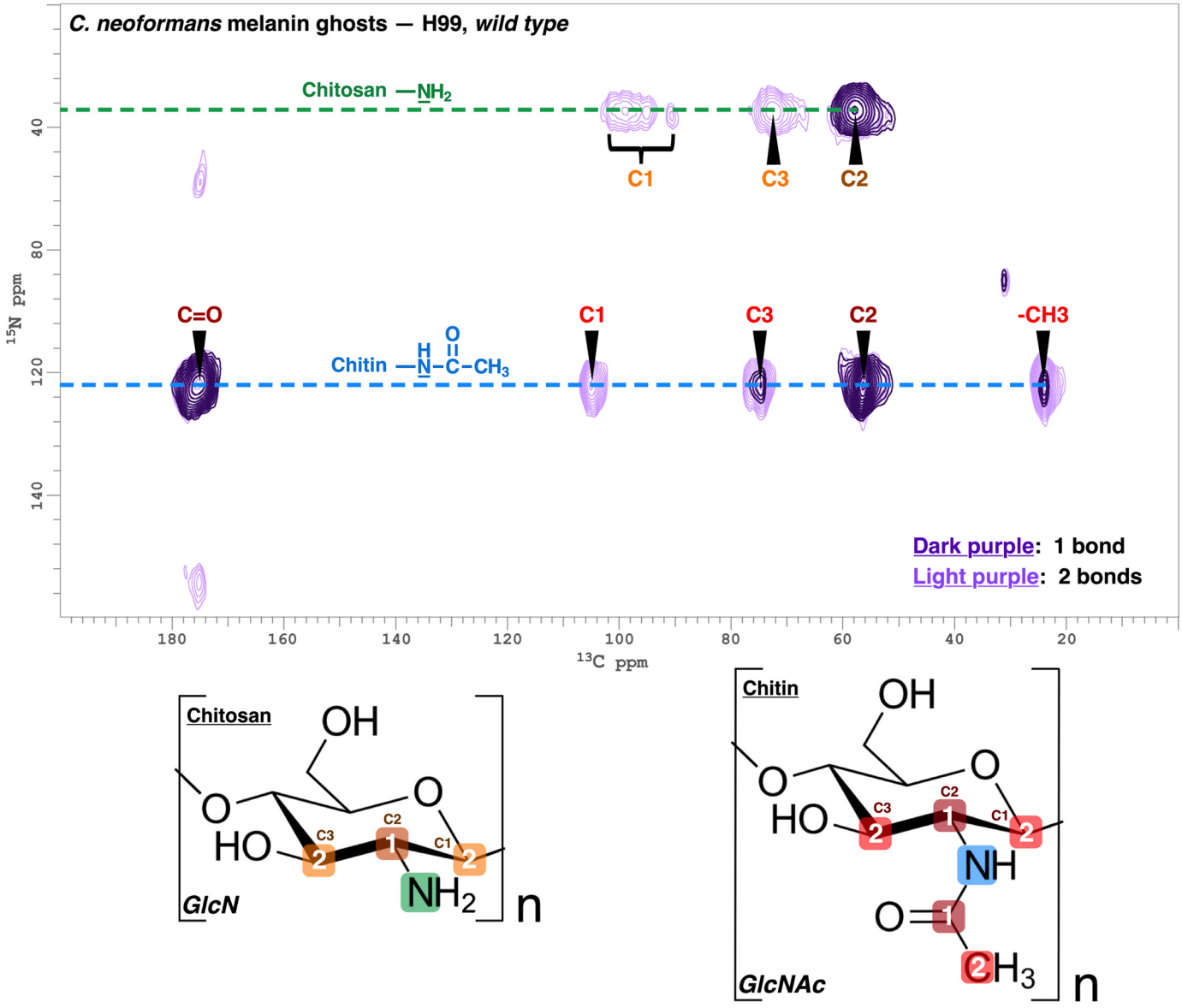

Figure 6. *C. neoformans* H99 melanin ghosts contain highly deacetylated chitosan. 2D ^{13}C-^{15}N TEDOR spectra of *C. neoformans* H99 melanin ghosts generated from cell cultures containing D-[U-$^{13}C_6$]glucose and [^{15}N]glycine as the sole carbon and nitrogen sources, respectively. Coherence transfer periods of 1.40 and 4.00 ms were used in separate experiments to obtain proximal carbon-nitrogen pairs separated by distances corresponding to ~1 bond length (*dark purple contours*) and ~2 bond lengths (*light purple contours*). The *boxed numbers* displayed on the chitin GlcNAc and chitosan glucosamine (*GlcN*) monomeric units denote the number of bonds between each ^{13}C-^{15}N nuclear pair.

Depending on the experimental parameters, the TEDOR contour plot displays proximal ^{13}C-^{15}N pairs located within selected distance ranges up to 5–6 Å. We acquired two complementary spectra that distinguished correlations involving ^{13}C-^{15}N nuclei with intervening distances corresponding to 1–2 bonds from longer-range pairs at distances up to 3 bonds. The short-distance melanin ghost 2D TEDOR plot (Fig. 6, *dark purple contours*) displayed three prominent cross-peaks attributable to proximal ^{13}C-^{15}N pairs (that are also directly bonded in the structures) in chitinous polysaccharides: the amide nitrogen of chitin is covalently linked to the C2 ring carbon (55 ppm ^{13}C × 123 ppm ^{15}N) and also to the carbonyl carbon of the acetyl group (174 × 123), and the amine nitrogen of chitosan is linked to the C2 ring carbon (57 × 35). The correlations displayed in the long-distance TEDOR spectrum of melanin ghosts (Fig. 6, *light purple contours*) further substantiate identification of the two principal nitrogenous constituents as chitin and chitosan: three additional cross-peaks involving the 123-ppm chitin amide nitrogen are unambiguously identifiable as intramolecular correlations with the methyl carbon of the acetyl group (24 × 123), C1 (104 × 123), and C3 ring carbons (73 × 123), respectively, each located 2 bonds away. Similarly, correlations between the chitosan amino nitrogen at 35 ppm are observed with C3 (72 × 35) and with C1 carbons situated in slightly different chemical environments (~90–100 × 35).

Although chitosan is often referred to as the deacetylated form of chitin, it would more accurately be classified as a binary heteropolysaccharide, because a percentage of the glucosamine residues remain acetylated (52). The C1 carbon participates in forming the glycosidic bond that links two adjacent monosac-

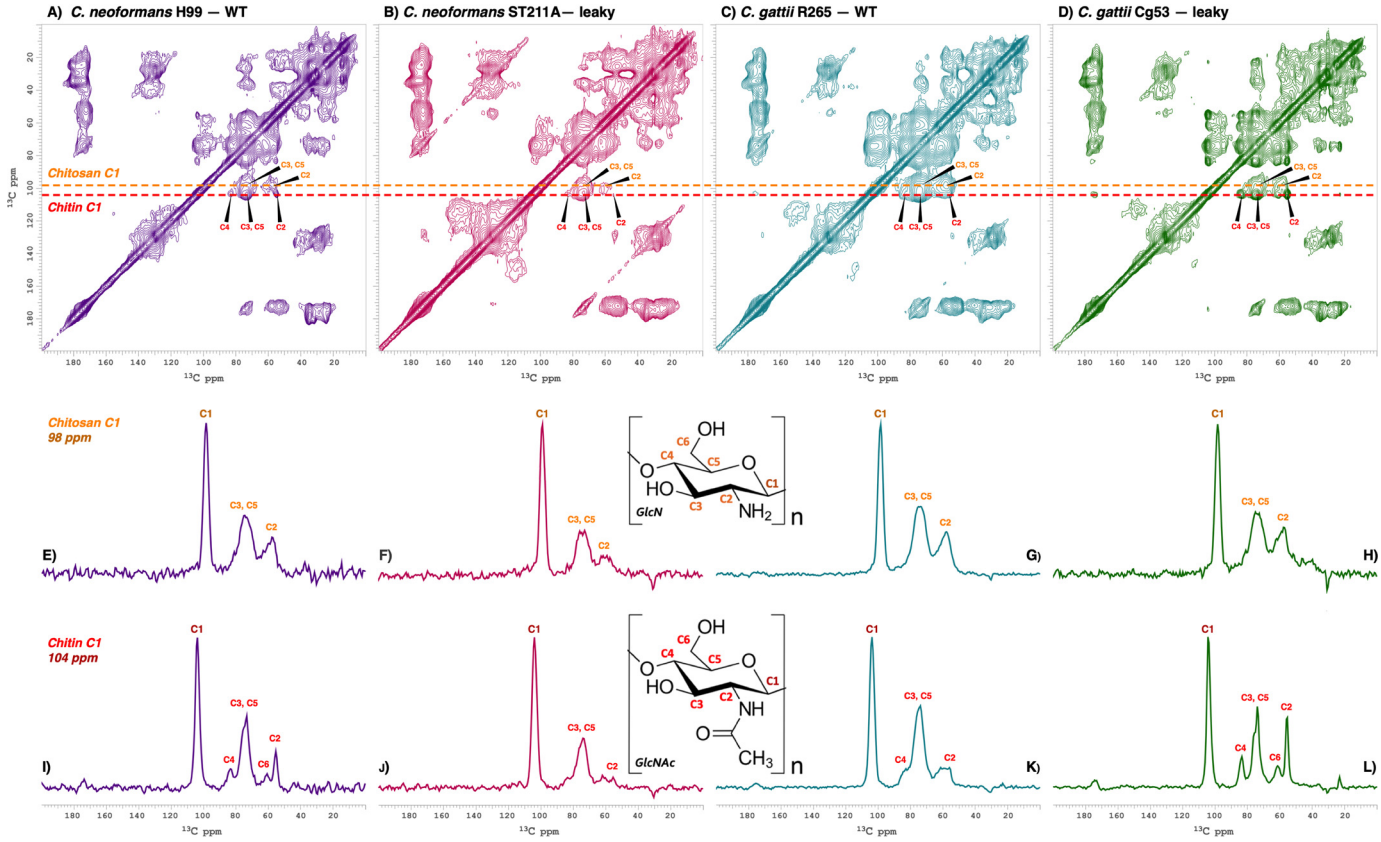

Figure 7. Cell-wall chitin flexibility is augmented in *C. neoformans* and *C. gattii* leaky mutant strain melanin ghosts. *Top row*, 2D ^{13}C-^{13}C DARR spectra (50-ms mixing time) of melanin ghosts generated from cell cultures containing D-[U-$^{13}C_6$]glucose as the sole carbon source. Cross-peaks represent proximal carbon pairs separated by distances corresponding to ~1 bond length. *Middle row*, 98-ppm cross-sections displaying chitosan C1 correlations. *Bottom row*, 104-ppm cross-sections displaying chitin C1 correlations. *A*, *E*, and *I*, *C. neoformans* H99 (WT). *B*, *F*, and *J*, *C. neoformans* ST211A (leaky). *C*, *G*, and *K*, *C. gattii* R265 (WT). *D*, *H*, and *L*, *C. gattii* Cg53 (leaky). The vertical scale of the 2D spectra was adjusted such that all significant cross-peaks are visible, and the same numbers of contours are displayed for the carbonyl resonance at 173 ppm. The 1D cross-sections were adjusted by setting the largest peak to full scale.

charide units; consequently, its chemical shift is influenced by the acetylation state of the succeeding residue and can provide information about the number and distribution of acetylated units within a chitin/chitosan polymer. The chitosan C1 correlations we observe in the TEDOR spectrum have carbon chemical shift values that span a 10-ppm range of upfield values below 100 ppm (Fig. 6), consistent with a highly deacetylated chitosan in which the glucosamine units have slightly different magnetic environments, depending on their proximity to sparse acetylated units with a "nonsequential random distribution" (52–54). These findings imply that the chitinous material in *C. neoformans* melanin ghosts comprises distinct polymers of GlcNAc (chitin) and glucosamine (chitosan), suggesting the possibility that they originate from different regions of the cell wall and play contrasting roles in the deposition of melanin pigments.

Melanin retention is associated with the flexibility of the cell-wall polysaccharide network

Thus far, a substantial body of evidence from our group and others has indicated that the cell-wall balance between chitin and chitosan directly influences the retention of melanin pigments (38, 39, 42). However, the possible changes in macromolecular architecture or chitin-chitosan arrangements that could promote or inhibit pigment retention have not been explored. To compare the molecular-level structural features of the chitin-chitosan network within the melanized cell walls of *C. neoformans* and *C. gattii*, including cells from both parent and "leaky" mutant strains, we examined the [U-^{13}C]glucose-enriched ghost samples using the 2D ^{13}C-^{13}C dipolar assisted rotation recoupling (DARR) solid-state NMR experiment. The parameters were optimized to detect proximal pairs of ^{13}C-^{13}C nuclei separated by distances corresponding to ~1 bond length.

To analyze the DARR contour plots in Fig. 7, we followed a roadmap to key ^{13}C chemical shift assignments that was provided by the ^{13}C-^{15}N TEDOR data of Fig. 6. Thus, the TEDOR spectra of U-^{13}C,^{15}N-enriched *C. neoformans* H99 melanin ghosts served to distinguish chitosan from the numerous other carbon-containing moieties in the [U-^{13}C]glucose-enriched DARR spectra: whereas the majority of polysaccharides have C1 ring carbons that resonate at 100–105 ppm, the C1 carbon chemical shift observed for chitosan reflects the highly deacetylated form of this polymer. As noted above, this value can vary between 90 and 100 ppm according to the acetylation state of its adjacent sugar units. The corresponding cross-peaks in the ^{13}C-^{13}C DARR spectrum can then be taken to correlate with proximal ring carbons located 1 bond (C1–C2, 98 × 57 ppm) or 2 bonds (C1–C3, 98 × 73; C1–C5, 98 × 75 ppm) apart (Fig. 7, *A–D*).

Although a common set of intramolecular correlations involving the chitosan C1 ring carbon was displayed in the ^{13}C-^{13}C DARR plots of the melanin ghost samples isolated from all strains, the relative signal intensities of the cross-peaks with respect to their parent diagonal peaks varied noticeably among the four spectra. Strong signals signify large dipole-dipole interactions between a pair of carbon nuclei; for interactions within a sugar ring that has defined intramolecular distances, they report on the degree to which the structure is well-defined. One-dimensional 98-ppm "slices" from the 2D DARR plots of ghost samples from each leaky strain were found to display significantly attenuated chitosan correlations relative to those observed in the spectra of their respective parent strains, demonstrating partial averaging of the pairwise dipolar interactions and attributable to molecular disorder and/or flexibility in the solid state (Fig. 7, *E–H*). The reduction in chitosan cross-peak intensity was especially pronounced in the spectrum of the *C. neoformans* ST211A leaky strain (Fig. 7*F*). Overall, however, the chitosan-rich composition of the *C. gattii* parent strain produced more robust chitosan correlations for R265 ghosts (Fig. 7*G*) compared with H99 samples (Fig. 7*E*). As a result, the chitosan cross-peak signal intensities were rendered similar for *C. neoformans* H99 (Fig. 7*E*) and *C. gattii* leaky Cg53 ghosts (Fig. 7*H*), suggesting that the degree of disorder associated with the leaky phenotype is strain-specific with respect to this polysaccharide constituent.

In contrast to the broad and poorly resolved signals of chitosan, the cross-peaks involving chitin were sharp and well-resolved, exhibiting numerous proximal ^{13}C-^{13}C interactions that were most evident in comparisons of the representative one-dimensional (1D) cross-sections (Fig. 7, *I–L*). Strikingly, the C1 carbon of chitin resonates at ~104 ppm; the peaks displayed in the corresponding 1D cross-section of the DARR spectrum are assigned to ring carbons located at distances corresponding to as many as 3 bonds apart (C1–C2, 104 × 56 ppm; C1–C3, 104 × 74; C1–C4, 104 × 84; C1–C5, 104 × 76). In comparison, the 98-ppm cross-section representative of the correlations involving the chitosan C1 ring carbon displays relatively broader peaks and carbon pairs located at most 2 bonds apart. These spectral variations are likely due to differences in molecular mobility between the two polysaccharides; chitin has a semicrystalline structure and is intrinsically more rigid than chitosan (55).

As observed for the chitosan constituent, variations in the ^{13}C-^{13}C DARR results for chitin were observed between the *Cryptococcus* strains and as a function of whether the melanin ghosts displayed the leaky phenotype. However, the trends were opposite for the *C. neoformans* and *C. gattii* leaky mutants: attenuation for *C. neoformans* ST211A (Fig. 7*J*) and augmentation for *C. gattii* Cg53 (Fig. 7*L*). Once again, the degree of disorder associated with the leaky phenotype for this polysaccharide constituent was found to be strain-specific. Thus, the leaky phenotype is found to occur when chitin is either anomalously disordered (*C. neoformans*) or unusually ordered (*C. gattii).* Nonetheless, a common hallmark of leaky mutants from both strains is the observation of disparate line widths and cross-peak intensities for the chitin and chitosan constituents, suggesting a mismatch in their degrees of crystallinity or propensity for molecular flexibility.

Discussion

This work was conceived following a curious observation under the light microscope: a portion of melanized cells from *C. gattii* R265 appeared to have strikingly pigmented cell walls, a peculiarity not witnessed in melanized cells from *C. neoformans* (Fig. 1). Further comparison of these two strains revealed that *C. gattii* R265 melanized cell walls had a relatively homogeneous distribution of melanin pigments throughout and are structurally more compact than those of *C. neoformans* H99 (Fig. 2, *A* and *B*). We can attribute this finding to the substantially higher chitosan content of the R265 strain in analogy with prior findings by our group: *C. neoformans* H99 cells grown in the presence of GlcNAc had increased chitosan levels compared with nonsupplemented control cells and concurrently exhibited a more uniform arrangement of cell-wall pigments, possibly due to an increase in electrostatic charge interactions (56, 57) and/or covalent linkage (58, 59) between chitosan and the melanin polymer. However, in GlcNAc-supplemented *C. neoformans* H99 cells, these features were found to correlate with an increase in melanization, whereas the *C. gattii* R265 strain actually retained a slightly smaller amount of cell-wall melanin pigments than *C. neoformans* H99 (Fig. 4). Thus, it is likely that chitosan promotes the uniform distribution of pigments, in turn leading to a more melanin-dense cell wall, but that other factors are involved in determining the overall extent of melanin deposition.

In the first reports linking cell-wall morphology and integrity with melanization, Banks *et al.* (39) and Baker *et al.* (38) determined that, of the eight chitin synthase proteins (Chs1–8) coded for by *C. neoformans*, the chitin synthase 3 enzyme (Chs3) and its chitin synthase regulator protein (Csr2) are responsible for the production of cell-wall chitin, a substantial portion of which is deacetylated to chitosan by one or more of three chitin deacetylase proteins (Cda1, Cda2, and Cda3) with redundant activity. Cells from *C. neoformans chs3*Δ, *csr2*Δ, and *cda1*Δ/*cda2*Δ/*cda3*Δ deletion strains were found to have normal or increased chitin levels but significantly diminished chitosan content. The mutant strains also displayed phenotypic traits such as incomplete cell separation during budding, increased sensitivity to certain cell-wall stressors, and, most notably, the inability to retain cell-wall melanin pigments, suggesting that chitosan deficiency could result in aberrant melanization.

In contrast, there is only one report of a *C. gattii* leaky melanin strain, designated Cg53, which was generated by Walton *et al.* (40) using insertional mutagenesis and subsequently determined to bear a mutation in the gene that encodes for Chs3. Nevertheless, no follow-up studies were reported that examine the effect of this genetic mutation on *C. gattii* cell-wall structure or the composition of chitinous polysaccharides. The *C. neoformans* ST211A leaky strain was also identified by Walton *et al.* (40) and found to bear a frameshift mutation in the *CSR2* gene (GenBank™ accession number MK609896). Thus, ST211A is likely genetically equivalent to the *csr2*Δ strain first reported by Banks *et al.* (39), and Cg53 is the *C. gattii* analog of

the *C. neoformans chs3*Δ mutant, both of which have previously been determined to display strikingly similar phenotypic traits, including decreased production of chitosan. Our biochemical determination of chitinous polysaccharides revealed that both of these mutants indeed have significantly lower chitosan levels than their respective parent strains (Fig. 3, *A* and *B*). Although anticipated for *C. neoformans* ST211A, this is the first demonstration that the deletion of *CHS3* in *C. gattii* results in diminished chitosan content. Therefore, our findings indicate that chitosan deficiency contributes to the leaky melanin phenotype displayed by Cg53 and that the role of chitosan in the deposition and retention of cell-wall melanin pigments is conserved in these two *Cryptococcus* species.

A recent study of chitin and chitosan and the role of the chitin deacetylases in *C. gattii* (60) confirms our finding that there is increased chitosan in *C. gattii* compared with *C. neoformans*, and our results go further to demonstrate that the amount of chitin in both species is similar. What is puzzling from the *C. gattii* deacetylase study is that the R265 strain deleted for all three *CDA* genes did not leak melanin, despite having almost no chitosan, running counter to the interpretations in this paper. However, in *C. neoformans*, when the three deacetylases were deleted, the amount of chitin was substantially increased (38). The difference between the mutants with defects in *CHS3* or *CSR2* and a strain without deacetylases is that the deacetylase mutant strain still has its full complement of functional chitin synthases; the deacetylase mutant produces the same amount of chitin, but none of the chitin is deacetylated to chitosan, thus increasing the overall amount of chitin in the cell wall compared with WT. Therefore, it is possible that there are substantially increased chitin or other components in the R265 *cda1*Δ*cda2*Δ*cda3*Δ strain that change the architecture and/or the flexibility of the cell wall and thus allow the melanin to be retained.

Despite the undeniable importance of chitosan in the anchoring and arrangement of cell-wall melanin pigments, other nonpolysaccharide constituents are also likely to be involved. Prior work by our group has demonstrated that the fungal pigments present in *C. neoformans* "melanin ghost" samples are complexed with an intricate aliphatic scaffold that includes both polysaccharides and lipids (31, 32). The fact that these relatively labile moieties can withstand the enzymatically and chemically degradative purification process used to generate melanin ghosts suggests they have become intimately associated with the pigment during its transport and/or deposition into the cell wall and thus play an integral role in melanin assembly.

In the current work, our spectroscopic data verified that the melanin pigments produced by *C. gattii* are tightly associated with an aliphatic framework composed of the same cellular constituents as in *C. neoformans*. However, quantitative ssNMR analysis of [^{13}C]glucose-enriched melanin ghosts isolated from the leaky and parent strains of both species revealed significant disparities in the relative amounts of retained constituent types. Notably, the relative proportions of polysaccharides estimated by ssNMR for ghosts (Fig. 5*B*) follow the same trend as the total amounts of chitin plus chitosan determined by the MBTH assay in unmelanized cells (Fig. 3*A*). Thus, cells that produce less chitinous material do not seem to compensate for this "loss" by retaining a greater percentage of their polysaccharides when in their melanized state. Instead, *C. gattii* Cg53 is found to retain more lipids, such as long-chain fatty acids, compared with its parent strain, whereas *C. neoformans* ST211A retains relatively more "other" components compared with H99. A possible explanation for this finding is that *C. gattii* and *C. neoformans* leaky mutant strains activate different compensatory mechanisms leading to increased production of nonpolysaccharide constituents as a response to the reduced production of cell-wall chitin and chitosan. Nevertheless, because Cg53 and ST211A bear mutations in different genes (*CHS3* and *CSR2*, respectively), it is uncertain whether these outcomes are species-specific or due to different genetic mutations.

Whereas changes in cell-wall composition can have a drastic impact on melanization, the possible influence of altered cell-wall architecture, even among strains with similar chitin content, had been unexplored. Our 2D ssNMR spectroscopic data support the premise that the macromolecular arrangement and structure of the constituents comprising the cell-wall framework play key roles in cryptococcal melanin deposition.

First, 2D ^{13}C-^{15}N TEDOR spectra of *C. neoformans* H99 melanin ghosts displayed ^{13}C chemical shifts that implicated a highly deacetylated form of chitosan (Fig. 6), for which the few remaining acetylated units are distributed in a nonsequential manner (52–54). This carbon chemical shift information then allowed us to infer the presence of highly deacetylated chitosan in the 2D ^{13}C-^{13}C DARR spectra of melanin ghosts from all four fungal strains. In contrast, the chitosan produced by most organisms is only partially deacetylated, resulting in a copolymer that confers both rigidity and flexibility to cellular structures in which it is incorporated (61, 62). The fact that both *C. neoformans* and *C. gattii* were found to produce highly deacetylated chitosan could mean that, with hydrogen bonding between chitin and chitosan precluded, both of these *Cryptococcus* species achieve strengthening of their cell walls via an architecture that promotes pigment deposition.

Second, the spectral differences observed between the 2D ^{13}C-^{13}C DARR plots of leaky and parent strain melanin ghosts cannot be accounted for simply by disparities in cell-wall composition. Notably, the peaks corresponding to the intramolecular ^{13}C-^{13}C contacts within chitin were found to differ in line width and intensity between the leaky and parent strain of each species (Fig. 7). By comparing the 1D cross-sectional slices that display correlations involving the chitin C1 carbon, it is evident that the signal intensities observed for *C. neoformans* ST211A were significantly diminished compared with those of *C. neoformans* H99. Given similar chitin levels, we cannot attribute this observation to a reduction in chitin content. Instead, the diminished peak intensities likely arise from partial averaging of dipolar interactions between chitin carbons, signifying an increase in the flexibility and/or disorder of the chitin polymers. The spectral features corresponding to chitin carbons were additionally found to differ between the *C. gattii* Cg53 leaky mutant and its parent strain R265 despite their similar chitin content. In contrast to our findings with *C. neoformans*, the chitin peaks of Cg53 were observed to have greater intensities and reduced line widths compared with those displayed by R265, indicating an increase in rigidity and/or molecular order. Moreover, it is noteworthy that chitin correlations displayed by

the parent type of each species have intermediate intensities and line widths, which suggests the presence of polymers that are both amorphous and crystalline to some degree.

The simplest explanation for these results is that the genetic mutation carried by each leaky strain has a direct influence on the ultrastructure of the chitin produced. Importantly, although the two leaky strains have mutations in two distinct genes, the proteins encoded by these genes have been hypothesized to form a complex that produces the chitin that can be converted to chitosan (39). Therefore, the two leaky strains are likely interrupting the same biological process and should have very similar phenotypes. For example, it is likely that the mutation of *CHS3* in Cg53 results in increased production of chitin by one of the other chitin synthases it encodes for, as seen in *C. neoformans chs3*Δ mutants (39), which could in turn produce chitin polymers that have a greater propensity to form rigid and/or well-ordered crystalline microfibrils.

An alternative explanation is that the disparate compositional changes in nonchitin constituents exhibited by the respective leaky mutant strains impact chitin ultrastructure differentially. For example, the increased proportion of nonpolysaccharide and nonlipid "other" constituents retained by ST211A melanin ghosts, which are likely composed of bulky and rigid aromatic ring systems, could potentially disrupt the hydrogen bonding between individual chitin polymers and thus produce a relatively disordered architecture. In either case, the fact that the chitin produced by both *C. neoformans* and *C. gattii* parent strains appears to have a macromolecular arrangement with intermediate properties suggests a Goldilocks principle, whereby a "just right" balance of flexibility/disorder and rigidity/order is required for optimal cell-wall melanin pigment deposition and retention.

In summary, this study provides the first detailed compositional and structural analysis of melanized cell walls from the two most clinically relevant isolates of the *Cryptococcus* species complex: *C. neoformans* H99 and *C. gattii* R265. By leveraging the dependence of cryptococcal species on exogenous precursors for melanin synthesis and implementing ssNMR spectroscopy, we generated isotopically enriched melanin ghosts for which it could be determined that pigments produced by each *C. neoformans* and *C. gattii* preferentially associate with different proportions of chitinous polysaccharides and lipids during melanin assembly. In addition, we verified the role of chitosan as a critical component of the cell-wall scaffold that governs melanin deposition and retention in both cryptococcal species and represents a major insight for this field. Nonetheless, further studies using multiple strains from these two cryptococcal species are required for validation. Altogether, a better understanding of these fungal melanized cell-wall structures could support the development of new and highly selective antifungal drugs.

Experimental procedures

Cryptococcus strains and culture conditions

All strains used in the current study are listed in Table 1. Yeast cells were kept frozen in 20% glycerol stocks and subcultured into Sabouraud dextrose broth for 48 h at 30 °C prior to each experiment. The yeast cells were washed three times with Dulbecco's PBS (DPBS) with calcium and magnesium (Corning, Inc.) and counted using a hemocytometer. Cultures inoculated with 1×10^6 cells ml^{-1} (end concentration) were grown in minimal medium (MM) (29.4 mM KH_2PO_4, 10 mM $MgSO_4$, 13 mM glycine, 3 μM thiamine, 15 mM glucose, pH 5.5) at 30 °C and shaken at moderate speed (120 rpm) for periods of 4–10 days in separate experiments. Melanized yeast cells were produced by inoculating cells in MM containing 1 mM L-DOPA as the obligatory melanization precursor and using the same culture conditions listed above. In designated experiments, glucose and/or glycine were replaced by [U-$^{13}C_6$]glucose (catalog no. GLC-082, Omicron Biochemical, Inc.) and [^{15}N]glycine (catalog no. 299294, Sigma-Aldrich), respectively. Aliquots of each culture were collected for light microscopy and transmission EM.

Microscopic studies for cell body and capsule measurements

C. neoformans H99 and *C. gattii* R265 nonmelanized and melanized cells, grown for 4 or 7 days in separate experiments, were washed three times with DPBS. To determine cell body and capsule sizes by light microscopy, washed yeast cells were suspended in India ink and visualized under an Olympus AX70 microscope (Olympus America) using a ×40 objective. The cell body and capsule dimensions were calculated as done previously (42). For each condition, 150 cells were measured in two independent experiments.

Assessment of chitinous cell-wall constituents

Cellular chitin and chitosan of nonmelanized yeast cells were estimated as described previously (42). Briefly, each alkaline-extracted sample was divided into two aliquots: one aliquot was deacetylated with hydrochloric acid (HCl) to measure the total amount of glucosamine arising from chitin plus chitosan, and the second aliquot remained untreated to measure the glucosamine from chitosan only. The amount of chitin-derived glucosamine was determined by taking the difference between the two measurements. Each aliquot was treated with MBTH, which forms a complex with hexosamines (amino sugars) under mildly acid conditions. The intense blue color yielded by this reaction was recorded at 650 nm. The amount of hexosamine in each sample was determined by comparison with a standard curve prepared from a 1 mM GlcNAc stock.

Transmission EM

Aliquots from *C. neoformans* H99 and *C. gattii* R265 melanized yeast cells were washed, adjusted to 1×10^6 cell ml^{-1} in DPBS, and fixed overnight with the same volume of 2.5% (v/v) glutaraldehyde, 3 mM $MgCl_2$ in 0.1 M sodium cacodylate buffer (pH 7.2) at 4 °C. After rinsing with buffer, cells were processed with 0.8% potassium ferrocyanide reduced with 1% OsO_4, serially dehydrated in a graded series of ethanol, and embedded in Eponate 12 (Ted Pella) resin. Ultrathin sections were obtained and stained with 2% uranyl acetate in 50% methanol, followed by lead citrate for examination with a Philips/FEI Bio Twin CM120 transmission electron microscope at 80 kV. Images were captured with an AMT XR80 high-resolution (16-bit) 8-megapixel camera. Using ImageJ software (Fiji) (63), micrograph analyses of 10–18 cells (5 calculations/cell) per

Cryptococcus strain were performed to determine the melanized cell wall dimensions.

Melanin isolation for solid-state NMR

Cryptococcal cells cultured in MM containing the melanization precursor L-DOPA for 10 days were subjected to acid digestion in a procedure known as "melanin ghost" isolation, where cellular material is digested but the acid-resistant melanin remains assembled into a structure with the dimensions of the original cell (33). The protocol involved progressive enzymatic and chemical removal of cell-wall polysaccharides, proteins, and lipids. All samples were extensively dialyzed against distilled water and subsequently lyophilized for 3 days before use.

ssNMR spectroscopy

Solid-state NMR measurements were carried out on a Varian (Agilent) DirectDrive2 (DD2) instrument operating at a ^{1}H frequency of 600 MHz. All data were acquired on ~5–10 mg of powdered samples using an MAS rate of 15.00 ± 0.02 kHz at a spectrometer-set temperature of 25 °C and processed with 100–150 Hz of line broadening. The 1D ^{13}C DPMAS and 2D ^{13}C-^{13}C DARR experiments were conducted on a 1.6-mm T3 HXY fastMAS probe (Agilent Technologies, Santa Clara, CA) with 90° pulse lengths of 1.2 and 1.4 μs for ^{1}H and ^{13}C, respectively, and 104-kHz heteronuclear decoupling using the small phase incremental alternation pulse sequence (SPINAL) during signal acquisition. To estimate the relative amounts of carbon-containing constituents in melanin ghost samples, 1D ^{13}C DPMAS experiments were performed with long (50-s) recycle delays to obtain quantitatively reliable signal intensities that allowed the integration of defined spectral regions using the GNU image manipulation program (GIMP). In 2D ^{13}C-^{13}C DARR experiments, the initial magnetization transfer from ^{1}H to ^{13}C was accomplished during a 1.5-ms cross-polarization period with a 10% linearly ramped radiofrequency field (rf) of 191 kHz for ^{1}H and a 179-kHz constant rf for ^{13}C. Proton irradiation with an rf of 16 kHz was applied during the 50-ms field-assisted diffusion mixing period. The 1D ^{15}N cross-polarization magic angle spinning (CPMAS) and 2D ^{13}C-^{15}N TEDOR experiments were run on a 3.2-mm T3 HXY MAS probe (Agilent Technologies, Santa Clara, CA) with 90° pulse lengths of 2.6, 4.0, and 4.5 μs for ^{1}H, ^{13}C, and ^{15}N, respectively, and 48-kHz SPINAL decoupling during acquisition. In the 1D ^{15}N CPMAS experiments, ^{1}H-^{15}N transfer was accomplished during a 2-ms period with a 10% linearly ramped rf of 66 kHz for ^{1}H and a 56-kHz constant rf for ^{15}N. In the 2D ^{13}C-^{15}N TEDOR experiments, the initial ^{1}H to ^{13}C transfer was accomplished during a 1.0-ms cross-polarization period with a 10% linearly ramped rf of 85 kHz for ^{1}H and a 63-kHz constant rf for ^{13}C. Coherence transfer periods of 1.40 and 4.00 ms were used in separate experiments to obtain ^{13}C-^{15}N correlations corresponding to approximately 1- and 2-bond distances, respectively.

Statistical analyses

Statistical analyses were performed using GraphPad Prism version 8.00 for Mac OS X (GraphPad Software, San Diego, CA). The 90–95% confidence interval was determined for each set of results.

Author contributions—C. C., E. C., R. P.-R., J. K. L., A. C., and R. E. S. conceptualization; C. C., E. C., M. S. F., R. P.-R., S. C., R. J. C., J. K. L., A. C., and R. E. S. formal analysis; C. C., E. C., M. S. F., R. P.-R., S. C., R. J. C., J. K. L., A. C., and R. E. S. validation; C. C., E. C., M. S. F., R. P.-R., S. C., and R. J. C. investigation; C. C., E. C., J. K. L., A. C., and R. E. S. visualization; C. C., E. C., M. S. F., R. P.-R., S. C., R. J. C., J. K. L., A. C., and R. E. S. methodology; C. C., E. C., J. K. L., A. C., and R. E. S. writing-original draft; C. C., E. C., J. K. L., A. C., and R. E. S. project administration; C. C., E. C., M. S. F., R. P.-R., S. C., R. J. C., J. K. L., A. C., and R. E. S. writing-review and editing; J. K. L., A. C., and R. E. S. supervision.

Acknowledgments—We thank Alexander Idnurm (Mycology Laboratory, University of Melbourne) for the kind gift of C. neoformans strain ST211A and Barbara Smith (Microscopy Facility, School of Medicine, Johns Hopkins University) for her expertise and technical assistance with transmission EM. We also thank Hsin Wang (City College, CUNY) and Van Chanh Phan (Hostos College, CUNY) for the development of NMR programs and technical support. The 600-MHz NMR facilities used in this work are operated by City College and the CUNY Institute for Macromolecular Assemblies, with additional infrastructural support provided by National Institutes of Health Grant 3G12MD007603-30S2 from the National Institute on Minority Health and Health Disparities of the National Institutes of Health.

References

1. Walker, L., Sood, P., Lenardon, M. D., Milne, G., Olson, J., Jensen, G., Wolf, J., Casadevall, A., Adler-Moore, J., and Gow, N. A. R. (2018) The viscoelastic properties of the fungal cell wall allow traffic of AmBisome as intact liposome vesicles. *MBio* **9,** e02383-17 CrossRef Medline
2. Latgé, J. P., and Beauvais, A. (2014) Functional duality of the cell wall. *Curr. Opin. Microbiol.* **20,** 111–117 CrossRef Medline
3. Perez, P., and Ribas, J. C. (2013) Fungal cell wall analysis. In *Laboratory Protocols in Fungal Biology* (Gupta, V., Tuohy, M., Ayyachamy, M., Turner, K., and O'Donovan, A., eds) pp. 175–196, Springer, New York
4. Lesage, G., and Bussey, H. (2006) Cell wall assembly in *Saccharomyces cerevisiae*. *Microbiol. Mol. Biol. Rev.* **70,** 317–343 CrossRef Medline
5. Gow, N. A. R., Latge, J. P., and Munro, C. A. (2017) The fungal cell wall: structure, biosynthesis, and function. *Microbiol. Spectr.* **5** CrossRef Medline
6. Free, S. J. (2013) Fungal cell wall organization and biosynthesis. *Adv. Genet.* **81,** 33–82 CrossRef Medline
7. Agustinho, D. P., Miller, L. C., Li, L. X., and Doering, T. L. (2018) Peeling the onion: the outer layers of *Cryptococcus neoformans*. *Mem. Inst. Oswaldo Cruz* **113,** e180040 CrossRef Medline
8. Perez, P., and Ribas, J. C. (2017) Fission yeast cell wall analysis. *Cold Spring Harb. Protoc.* **2017,** pdb.top079897 CrossRef Medline
9. Doering, T. L. (2009) How sweet it is! Cell wall biogenesis and polysaccharide capsule formation in *Cryptococcus neoformans*. *Annu. Rev. Microbiol.* **63,** 223–247 CrossRef Medline
10. Kwon-Chung, K. J., Bennett, J. E., Wickes, B. L., Meyer, W., Cuomo, C. A., Wollenburg, K. R., Bicanic, T. A., Castaneda, E., Chang, Y. C., Chen, J., Cogliati, M., Dromer, F., Ellis, D., Filler, S. G., Fisher, M. C., *et al.* (2017) The case for adopting the "species complex" nomenclature for the etiologic agents of cryptococcosis. *mSphere* **2,** e00357-16 CrossRef Medline
11. Chowdhary, A., Rhandhawa, H. S., Prakash, A., and Meis, J. F. (2012) Environmental prevalence of *Cryptococcus neoformans* and *Cryptococcus gattii* in India: an update. *Crit. Rev. Microbiol.* **38,** 1–16 CrossRef Medline
12. Ellis, D. H., and Pfeiffer, T. J. (1990) Natural habitat of *Cryptococcus neoformans* var. gattii. *J. Clin. Microbiol.* **28,** 1642–1644 CrossRef Medline

13. Emmons, C. W. (1955) Saprophytic sources of *Cryptococcus neoformans* associated with the pigeon (*Columba livia*). *Am. J. Hyg.* **62,** 227–232 CrossRef Medline
14. Sorrell, T. C., Brownlee, A. G., Ruma, P., Malik, R., Pfeiffer, T. J., and Ellis, D. H. (1996) Natural environmental sources of *Cryptococcus neoformans* var. gattii. *J. Clin. Microbiol.* **34,** 1261–1263 CrossRef Medline
15. May, R. C., Stone, N. R., Wiesner, D. L., Bicanic, T., and Nielsen, K. (2016) Cryptococcus: from environmental saprophyte to global pathogen. *Nat. Rev. Microbiol.* **14,** 106–117 CrossRef Medline
16. Findley, K., Rodriguez-Carres, M., Metin, B., Kroiss, J., Fonseca, A., Vilgalys, R., and Heitman, J. (2009) Phylogeny and phenotypic characterization of pathogenic *Cryptococcus* species and closely related saprobic taxa in the Tremellales. *Eukaryot. Cell* **8,** 353–361 CrossRef Medline
17. Xu, J., Vilgalys, R., and Mitchell, T. G. (2000) Multiple gene genealogies reveal recent dispersion and hybridization in the human pathogenic fungus *Cryptococcus neoformans*. *Mol. Ecol.* **9,** 1471–1481 CrossRef Medline
18. Casadevall, A., Freij, J. B., Hann-Soden, C., and Taylor, J. (2017) Continental drift and speciation of the *Cryptococcus neoformans* and *Cryptococcus gattii* species complexes. *mSphere* **2,** e00103-17 CrossRef Medline
19. Freij, J. B., Fu, M. S., De Leon Rodriguez, C. M., Dziedzic, A., Jedlicka, A. E., Dragotakes, Q., Rossi, D. C. P., Jung, E. H., Coelho, C., and Casadevall, A. (2018) Conservation of intracellular pathogenic strategy among distantly related cryptococcal species. *Infect. Immun.* **86,** e00946-17 CrossRef Medline
20. Gerstein, A. C., and Nielsen, K. (2017) It's not all about us: evolution and maintenance of *Cryptococcus virulence* requires selection outside the human host. *Yeast* **34,** 143–154 CrossRef Medline
21. Eisenman, H. C., and Casadevall, A. (2012) Synthesis and assembly of fungal melanin. *Appl. Microbiol. Biotechnol.* **93,** 931–940 CrossRef Medline
22. Zaragoza, O., Rodrigues, M. L., De Jesus, M., Frases, S., Dadachova, E., and Casadevall, A. (2009) The capsule of the fungal pathogen *Cryptococcus neoformans*. *Adv. Appl. Microbiol.* **68,** 133–216 CrossRef Medline
23. White, L. P. (1958) Melanin: a naturally occurring cation exchange material. *Nature* **182,** 1427–1428 CrossRef Medline
24. Enochs, W. S., Nilges, M. J., and Swartz, H. M. (1993) A standardized test for the identification and characterization of melanins using electron paramagnetic resonance (EPR) spectroscopy. *Pigment Cell Res.* **6,** 91–99 CrossRef Medline
25. Nosanchuk, J. D., and Casadevall, A. (2006) Impact of melanin on microbial virulence and clinical resistance to antimicrobial compounds. *Antimicrob. Agents Chemother.* **50,** 3519–3528 CrossRef Medline
26. Nosanchuk, J. D., and Casadevall, A. (2003) The contribution of melanin to microbial pathogenesis. *Cell Microbiol.* **5,** 203–223 CrossRef Medline
27. Mednick, A. J., Nosanchuk, J. D., and Casadevall, A. (2005) Melanization of *Cryptococcus neoformans* affects lung inflammatory responses during cryptococcal infection. *Infect. Immun.* **73,** 2012–2019 CrossRef Medline
28. Williamson, P. R., Wakamatsu, K., and Ito, S. (1998) Melanin biosynthesis in *Cryptococcus neoformans*. *J. Bacteriol.* **180,** 1570–1572 CrossRef Medline
29. Liu, L., Wakamatsu, K., Ito, S., and Williamson, P. R. (1999) Catecholamine oxidative products, but not melanin, are produced by *Cryptococcus neoformans* during neuropathogenesis in mice. *Infect. Immun.* **67,** 108–112 CrossRef Medline
30. Zhong, J., Frases, S., Wang, H., Casadevall, A., and Stark, R. E. (2008) Following fungal melanin biosynthesis with solid-state NMR: biopolymer molecular structures and possible connections to cell-wall polysaccharides. *Biochemistry* **47,** 4701–4710 CrossRef Medline
31. Chatterjee, S., Prados-Rosales, R., Itin, B., Casadevall, A., and Stark, R. E. (2015) Solid-state NMR reveals the carbon-based molecular architecture of *Cryptococcus neoformans* fungal eumelanins in the cell wall. *J. Biol. Chem.* **290,** 13779–13790 CrossRef Medline
32. Chatterjee, S., Prados-Rosales, R., Tan, S., Phan, V. C., Chrissian, C., Itin, B., Wang, H., Khajo, A., Magliozzo, R. S., Casadevall, A., and Stark, R. E. (2018) The melanization road more traveled by: precursor substrate effects on melanin synthesis in cell-free and fungal cell systems. *J. Biol. Chem.* **293,** 20157–20168 CrossRef Medline
33. Chatterjee, S., Prados-Rosales, R., Frases, S., Itin, B., Casadevall, A., and Stark, R. E. (2012) Using solid-state NMR to monitor the molecular consequences of *Cryptococcus neoformans* melanization with different catecholamine precursors. *Biochemistry* **51,** 6080–6088 CrossRef Medline
34. Wang, Z., Zheng, L., Hauser, M., Becker, J. M., and Szaniszlo, P. J. (1999) WdChs4p, a homolog of chitin synthase 3 in *Saccharomyces cerevisiae,* alone cannot support growth of *Wangiella* (*Exophiala*) *dermatitidis* at the temperature of infection. *Infect. Immun.* **67,** 6619–6630 Medline
35. Bull, A. T. (1970) Chemical composition of wild-type and mutant *Aspergillus nidulans* cell walls: the nature of polysaccharide and melanin constituents. *J. Gen. Microbiol.* **63,** 75–94 CrossRef Medline
36. Walker, C. A., Gómez, B. L., Mora-Montes, H. M., Mackenzie, K. S., Munro, C. A., Brown, A. J., Gow, N. A., Kibbler, C. C., and Odds, F. C. (2010) Melanin externalization in *Candida albicans* depends on cell wall chitin structures. *Eukaryot. Cell* **9,** 1329–1342 CrossRef Medline
37. Stavenga, D. G., Leertouwer, H. L., Hariyama, T., De Raedt, H. A., and Wilts, B. D. (2012) Sexual dichromatism of the damselfly *Calopteryx japonica* caused by a melanin-chitin multilayer in the male wing veins. *PLoS ONE* **7,** e49743 CrossRef Medline
38. Baker, L. G., Specht, C. A., Donlin, M. J., and Lodge, J. K. (2007) Chitosan, the deacetylated form of chitin, is necessary for cell wall integrity in *Cryptococcus neoformans*. *Eukaryot. Cell* **6,** 855–867 CrossRef Medline
39. Banks, I. R., Specht, C. A., Donlin, M. J., Gerik, K. J., Levitz, S. M., and Lodge, J. K. (2005) A chitin synthase and its regulator protein are critical for chitosan production and growth of the fungal pathogen *Cryptococcus neoformans*. *Eukaryot. Cell* **4,** 1902–1912 CrossRef Medline
40. Walton, F. J., Idnurm, A., and Heitman, J. (2005) Novel gene functions required for melanization of the human pathogen *Cryptococcus neoformans*. *Mol. Microbiol.* **57,** 1381–1396 CrossRef Medline
41. Baker, L. G., Specht, C. A., and Lodge, J. K. (2009) Chitinases are essential for sexual development but not vegetative growth in *Cryptococcus neoformans*. *Eukaryot. Cell* **8,** 1692–1705 CrossRef Medline
42. Camacho, E., Chrissian, C., Cordero, R. J. B., Liporagi-Lopes, L., Stark, R. E., and Casadevall, A. (2017) *N*-Acetylglucosamine affects *Cryptococcus neoformans* cell-wall composition and melanin architecture. *Microbiology* **163,** 1540–1556 CrossRef Medline
43. Tsirilakis, K., Kim, C., Vicencio, A. G., Andrade, C., Casadevall, A., and Goldman, D. L. (2012) Methylxanthine inhibit fungal chitinases and exhibit antifungal activity. *Mycopathologia* **173,** 83–91 CrossRef Medline
44. Fraser, J. A., Giles, S. S., Wenink, E. C., Geunes-Boyer, S. G., Wright, J. R., Diezmann, S., Allen, A., Stajich, J. E., Dietrich, F. S., Perfect, J. R., and Heitman, J. (2005) Same-sex mating and the origin of the Vancouver Island *Cryptococcus gattii* outbreak. *Nature* **437,** 1360–1364 CrossRef Medline
45. Ngamskulrungroj, P., and Meyer, W. (2009) Melanin production at 37 °C is linked to the high virulent *Cryptococcus gattii* Vancouver Island outbreak genotype VGIIa. *Aust. Mycol.* **28,** 9–15
46. Ngamskulrungroj, P., Serena, C., Gilgado, F., Malik, R., and Meyer, W. (2011) Global VGIIa isolates are of comparable virulence to the major fatal *Cryptococcus gattii* Vancouver Island outbreak genotype. *Clin. Microbiol. Infect.* **17,** 251–258 CrossRef Medline
47. Polacheck, I., Platt, Y., and Aronovitch, J. (1990) Catecholamines and virulence of *Cryptococcus neoformans*. *Infect. Immun.* **58,** 2919–2922 CrossRef Medline
48. Watson, H. R., Apperley, D. C., Dixon, D. P., Edwards, R., and Hodgson, D. R. (2009) An efficient method for ^{15}N-labeling of chitin in fungi. *Biomacromolecules* **10,** 793–797 CrossRef Medline
49. Heux, L., Brugnerotto, J., Desbrières, J., Versali, M. F., and Rinaudo, M. (2000) Solid state NMR for determination of degree of acetylation of chitin and chitosan. *Biomacromolecules* **1,** 746–751 CrossRef Medline
50. Jaroniec, C. P., Filip, C., and Griffin, R. G. (2002) 3D TEDOR NMR experiments for the simultaneous measurement of multiple carbon-nitrogen distances in uniformly ^{13}C,^{15}N-labeled solids. *J. Am. Chem. Soc.* **124,** 10728–10742 CrossRef Medline
51. Hing, A. W., Vega, S., and Schaefer, J. (1993) Measurement of heteronuclear dipolar coupling by transferred-echo double-resonance NMR. *J. Magn. Reson. Ser. A* **103,** 151–162 CrossRef

52. Vårum, K. M., Anthonsen, M. W., Grasdalen, H., and Smidsrød, O. (1991) Determination of the degree of *N*-acetylation and the distribution of *N*-acetyl groups in partially *N*-deacetylated chitins (chitosans) by high-field n.m.r. spectroscopy. *Carbohydr. Res.* **211,** 17–23 CrossRef Medline
53. Vårum, K. M., Anthonsen, M. W., Grasdalen, H., and Smidsrød, O. (1991) ^{13}C-n.m.r. studies of the acetylation sequences in partially *N*-deacetylated chitins (chitosans). *Carbohydr. Res.* **217,** 19–27 CrossRef Medline
54. Weinhold, M. X., Sauvageau, J. C. M., Kumirska, J., and Thöming, J. (2009) Studies on acetylation patterns of different chitosan preparations. *Carbohydr. Polym.* **78,** 678–684 CrossRef
55. Oh, D. X., Cha, Y. J., Nguyen, H. L., Je, H. H., Jho, Y. S., Hwang, D. S., and Yoon, D. K. (2016) Chiral nematic self-assembly of minimally surface damaged chitin nanofibrils and its load bearing functions. *Sci. Rep.* **6,** 23245 CrossRef Medline
56. Nosanchuk, J. D., and Casadevall, A. (1997) Cellular charge of *Cryptococcus neoformans*: contributions from the capsular polysaccharide, melanin, and monoclonal antibody binding. *Infect. Immun.* **65,** 1836–1841 CrossRef Medline
57. Quemeneur, F., Rinaudo, M., and Pépin-Donat, B. (2008) Influence of molecular weight and pH on adsorption of chitosan at the surface of large and giant vesicles. *Biomacromolecules* **9,** 396–402 CrossRef Medline
58. Zhang, Y., Thomas, Y., Kim, E., and Payne, G. F. (2012) pH- and voltage-responsive chitosan hydrogel through covalent cross-linking with catechol. *J. Phys. Chem. B* **116,** 1579–1585 CrossRef Medline
59. Zhu, X., and Williamson, P. R. (2004) Role of laccase in the biology and virulence of *Cryptococcus neoformans*. *FEMS Yeast Res.* **5,** 1–10 CrossRef Medline
60. Lam, W. C., Upadhya, R., Specht, C. A., Ragsdale, A. E., Hole, C. R., Levitz, S. M., and Lodge, J. K. (2019) Chitosan biosynthesis and virulence in the human fungal pathogen *Cryptococcus gattii*. *mSphere* **4,** e00644-19 CrossRef Medline
61. Grifoll-Romero, L., Pascual, S., Aragunde, H., Biarnés, X., and Planas, A. (2018) Chitin deacetylases: structures, specificities, and biotech applications. *Polymers* (*Basel*) **10,** E352 Medline
62. Cui, J., Yu, Z., and Lau, D. (2016) Effect of acetyl group on mechanical properties of chitin/chitosan nanocrystal: a molecular dynamics study. *Int. J. Mol. Sci.* **17,** E61 CrossRef Medline
63. Schindelin, J., Arganda-Carreras, I., Frise, E., Kaynig, V., Longair, M., Pietzsch, T., Preibisch, S., Rueden, C., Saalfeld, S., Schmid, B., Tinevez, J. Y., White, D. J., Hartenstein, V., Eliceiri, K., Tomancak, P., and Cardona, A. (2012) Fiji: an open-source platform for biological-image analysis. *Nat. Methods* **9,** 676–682 CrossRef Medline
64. Toffaletti, D. L., Rude, T. H., Johnston, S. A., Durack, D. T., and Perfect, J. R. (1993) Gene transfer in *Cryptococcus neoformans* by use of biolistic delivery of DNA. *J. Bacteriol.* **175,** 1405–1411 CrossRef Medline
65. Fraser, J. A., Subaran, R. L., Nichols, C. B., and Heitman, J. (2003) Recapitulation of the sexual cycle of the primary fungal pathogen *Cryptococcus neoformans* var. gattii: implications for an outbreak on Vancouver Island, Canada. *Eukaryot. Cell* **2,** 1036–1045 CrossRef Medline

Melanin deposition in two *Cryptococcus* species depends on cell-wall composition and flexibility

Christine Chrissian, Emma Camacho, Man Shun Fu, Rafael Prados-Rosales, Subhasish Chatterjee, Radames J. B. Cordero, Jennifer K. Lodge, Arturo Casadevall and Ruth E. Stark

J. Biol. Chem. 2020, 295:1815-1828.
doi: 10.1074/jbc.RA119.011949 originally published online January 2, 2020
